

PACS numbers: 87.64.M – ; 78.67.Bf; 73.20.Mf
DOI: 10.1070/QE2008v038n06ABEH013831

Dynamic ultramicroscopy of laser-induced flows in colloidal solutions of plasmon-resonance particles

I.V. Fedosov, I.S. Nefedov, B.N. Khlebtsov, V.V. Tuchin

***Abstract*. A method is proposed for visualisation of the velocity fields of colloidal plasmon-resonance nanoparticles moving in a laser beam. The method uses the particle image velocimetry for processing ultramicroscopic images. Particles in a thick layer of colloidal solution are illuminated by a slit laser ultramicroscopic source with a large numerical aperture providing a high contrast of particle images and visualisation of the transverse velocity distribution in laser-induced flows with a high spatial resolution.**

Keywords: *ultramicroscope, particle image velocimetry, colloidal particles.*

1. Introduction

Molecular sensors, optical contrasting agents and means for therapeutic action based on noble metal colloidal particles find increasing applications in modern biology and medicine [1 – 3]. Due to a surface plasmon resonance at optical frequencies, these particles scatter and absorb light much stronger than other objects of similar size. The resonance frequency at which absorption and scattering of light by colloidal particles drastically increase is determined by the shape and size of particles. By synthesising particles in the form of spheres, spherical shells or rods and varying their size, the plasmon resonance can be easily tuned to any wavelength in the visible or IR spectral region [2, 3]. Plasmon-resonance particles tuned to specified wavelengths and containing active antibodies attached to them can be used as convenient optical markers for increasing the contrast of specific tissues and cells in microscopy, optical tomography and photothermal therapy of oncology diseases [3, 4].

Microscopic studies of the mechanisms of interaction of such markers with individual cells require the development of new methods for visualisation of colloidal particles and optical manipulation of them. Because the size of plasmon-resonance particles is an order of magnitude smaller than the wavelength of light, individual particles can be observed only by ultramicroscopy methods [5], which, however, do not allow their shape and size to be determined directly [2]. Methods of optical manipulation, which have been successfully used for two decades in biologic studies for capturing, confining, and moving microscopic objects [6, 7], are also inefficient in the case of metal colloidal particles. The capturing of particles by gradient optical traps weakens with decreasing particle size, while plasmon-resonance particles themselves are overheated in tightly focused laser beams [8]. To solve these problems, it is necessary to study in detail the interaction of colloidal particles with optical radiation fields.

We have used the method of particle image velocimetry (PIV) for visualisation of the velocity field of colloidal nanoparticles accelerated in a laser beam [9, 10]. Because nanoparticles were visualised by radiation of the accelerating laser, it was impossible, first, to observe the dynamics of particles outside the laser beam and, second, to study the three-dimensional velocity distribution in the laser beam.

At present, the three-dimensional velocity distribution in microscopic flows is studied with a high spatial resolution by PIV methods. The spatial resolution over depth is determined by the depth of focus of the objective of a microscope with a large numerical aperture. Information on the third coordinate of a particle in the flow is obtained by the methods of image convolution inversion [11, 12]. Both these approaches require the use of objectives with a high numerical aperture and, hence, with a very small operating interval, which complicates coupling a laser beam in a medium in studies of laser-induced flows.

In this paper, we describe the method for visualisation of laser-induced flows by using a slit laser ultramicroscope source for visualisation of colloidal particles, which provides a high resolution over depth even for objectives with a comparatively small numerical aperture.

2. Materials and methods

2.1 Ultramicroscopic visualisation of plasmon-resonance particles

The method for observation of particles of size smaller than the wavelength of visible light was proposed more than a hundred years ago and was called ultramicroscopy [5]. The

I.V. Fedosov, V.V. Tuchin Department of Optics and Medical Biophysics, N.G. Chernyshevsky Saratov State University, ul. Astrakhanskaya 83, 410012 Saratov, Russia; e-mail: fedosov_optics@mail.ru;
I.S. Nefedov SMARAD Department of Radio Science and Engineering, Helsinki University of Technology (TKK), P.O. 3000, FI-02015 TKK, Finland;
B.N. Khlebtsov Institute of Biochemistry and Physiology of Plants and Microorganisms, Russian Academy of Sciences, prosp. Entuziastov 13, 410049 Saratov, Russia

Received 20 February 2008; revision received 13 March 2008
Kvantovaya Elektronika **38** (6) 530 – 535 (2008)
Translated by M.N. Sapozhnikov

method is based on the illumination of the volume under study by a narrow light beam perpendicular to the observation direction. Radiation scattered by nanoparticles contained in the volume produces their images in the form of bright point sources against a dark background in the field of view of a microscope, which allows one to detect nanoparticles and measure their concentration. At present ultramicroscopy is widely used for studying various disperse and colloidal systems [13, 14] and in new methods of optical tomography of biological tissues [15].

Plasmon-resonance colloidal particles, in particular, biological markers are also visualised by other methods of dark-field microscopy by using specialised condensers, epiobjectives or frustrated total internal reflection effect [2]. However, these methods can be applied only for studying monolayers of colloidal particles deposited on a glass surface. An increase in the thickness of the colloidal solution under study severely reduces the image contrast due to the scattering of light by particles located outside the object plane of the microscope objective and multiple reflection of light in the volume under study and a condenser. Therefore, the most convenient method for observation of these particles suspended in a large liquid volume is classical slit ultramicroscopy based on the illumination of the volume under study by a plane light beam perpendicular to the observation direction.

The spatial resolution of an ultramicroscope is determined by the image size of particles, which can be treated as point sources. The image of a point source obtained with the help of the diffraction-limited objective of a microscope with a circular aperture has the form of an Airy circle with the diameter of the first diffraction maximum equal to [16]

$$d = 2.44\lambda(M+1)\tilde{f}, \tag{1}$$

where M is the objective magnification; λ is the light wavelength; and $\tilde{f}$ is the relative aperture of the microscope objective. For the objective producing the image of an object at infinity, the relative aperture is

$$\tilde{f} \approx \frac{1}{2}\left[\left(\frac{n}{\mathrm{NA}}\right)^2 - 1\right]^{1/2}, \tag{2}$$

where n is the refractive index of the medium in the object space and NA is the numerical aperture of the microscope objective.

2.2 Particle image velocimetry

The PIV method allows the accurate visualisation of the two-dimensional velocity fields of particles moving in liquid or gas flows [17]. The method is based on the recording of two successive images of particles moving in the flow. The field of view is divided into many identical regions (windows). The most probable local displacement $\Delta\boldsymbol{r}$ of particles within each window is found by estimating the cross correlation of the fragments of the first and second images corresponding to this window. If the instants of recording the first and second images are separated by the time interval Δt, the local velocity $\boldsymbol{u}$ of the flow is defined as the ratio of the measured displacement to this time interval:

$$\boldsymbol{u} = \frac{\Delta\boldsymbol{r}}{\Delta t}. \tag{3}$$

By repeating this procedure for all the windows, the two-dimensional field of local velocities of particles is obtained. The cross-correlation intensity function for the fragments of two successively recorded mages is usually estimated as [17]

$$\Phi_k(m,n) = \sum_{j=1}^{q}\sum_{i=1}^{p} f_k(i,j)g_k(i+m,j+n), \tag{4}$$

where $f_k(i,j)$ and $g_k(i,j)$ are the intensities of the kth fragments of the first and second images, respectively. Both fragments correspond to the same analysed region (window) of size $p \times q$ pixels. The function $\Phi_k(m,n)$ will have a maximum for m and n corresponding to the most probable displacement of particle images within the window being analysed. The dispersion of the estimate of $\Phi_k(m,n)$ depends on the noise in initial images, the displacement of particles due to the Brownian motion and the mean number of particles with the window being analysed.

To reduce the dispersion of the correlation function estimate in the study of stationary microscopic flows, a great number of image pairs are recorded successively. The correlation function is estimated for each window as the average of the estimates of correlation functions obtained for each pair of images. The position of the estimate maximum obtained in this way will correspond to the average displacement of particle during the observation time. This method was first proposed and demonstrated in [17].

Errors in the visualisation of colloidal particles are mainly caused by random thermal motion due to collisions of particles with liquid molecules, which is called the Brownian motion [18]. The dynamics of this process for time intervals Δt exceeding the inertial response time of particles is independent of the density of the liquid and particles suspended in it. The root-mean-square displacement of a particle caused by Brownian motion is proportional to $D\Delta t$, where D is the diffusion coefficient of particles. The diffusion coefficient for a spherical particle is determined by the expression [19]

$$D = \frac{kT}{3\pi\mu d_{\mathrm{p}}}, \tag{5}$$

where d_{p} is the particle diameter; k is the Boltzmann constant; T is the absolute temperature of the liquid; and μ is the dynamic viscosity of the liquid. As shown in [20], a random displacement of particles due to Brownian motion leads to the relative errors

$$\varepsilon_x = \frac{1}{u_x}\left(\frac{2D}{\Delta t}\right)^{1/2}, \quad \varepsilon_y = \frac{1}{u_y}\left(\frac{2D}{\Delta t}\right)^{1/2} \tag{6}$$

in the determination of the particle velocity, where u_x and u_y are the x and y components, respectively, of the particle velocity $\boldsymbol{u}$; and Δt is the time interval between the instants of recording the first and second images of the particle. Relations (6) allow one to estimate the minimal time interval Δt for which the errors in the determination of the particle velocity caused by Brownian motion do not exceed the specified values.

2.3 Experimental setup

Laser-induced flows of colloidal solutions of plasmon-resonance particles were studied in a specially designed

microcell (Fig. 1). Cell base (*2*) was made of a 1-mm-thick aluminium alloy plate having a cut closed from three sides by windows (*1*), (*3*), (*4*) made of 170-μm-thick cover glasses glued to the cell base with epoxy compound. The cell was filled, emptied, and rinsed through two metal capillaries (*5*) with the inner diameter 300 μm, which were glued to the side walls of the microcell. The radiation from a laser moving colloidal particles was coupled through front window (*1*). The ultramicroscopic illumination of a liquid volume by a plane laser beam was performed through rear window (*4*). The particles, whose images were formed by radiation scattered in direction (*8*), were observed through top window (*3*). The cell design excludes the formation of capillary flows caused by evaporation, while the metal base reduces the temperature gradient producing convective flows in the cell.

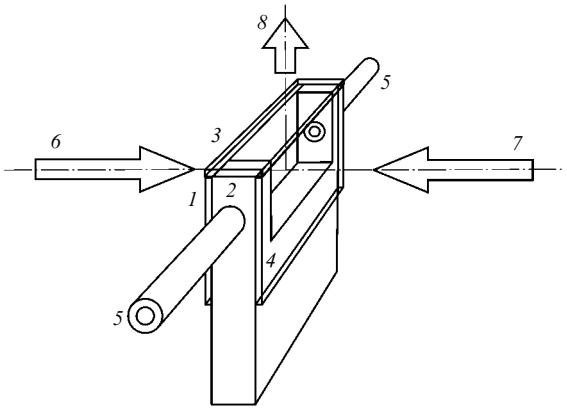

Figure 1. Scheme of a microcell: (*1*) front window; (*2*) base; (*3*) top window; (*4*) rear window; (*5*) capillary tubes; (*6*) direction of a force laser beam; (*7*) direction of an illuminating laser beam; (*8*) direction of scattered radiation forming particle images.

The ultramicroscopic system for studying the laser-induced dynamics of colloidal particles was developed based on a Biolam-M luminescence microscope (LOMO, Russia) (Fig. 2). The collimated beam from force laser (*1*) was expanded in telescopic system (*2*) and focused by objective (*3*) inside microcell (*4*) by passing through its front window. Force laser (*1*) in Fig. 2 was a 660-nm, 65-mW KLM 650-50 semiconductor laser (FTI-Optronik, Russia). The volume under study was illuminated through the rear window of the cell by laser (*19*) whose beam was formed by cylindrical lens (*17*) and microscope objective (*16*) and directed on telescopic slit aperture (*15*) of width 10 μm. The aperture image was projected inside the cell by objective (*11*). To exclude the damage of laser (*19*), the radiation from the force laser was suppressed with SZS 22 glass filter (*18*). Illuminating laser (*19*) in Fig. 2 was a diode-pumped 532-nm, 3-mW LCS-T-11 solid-state laser (Laser-Compact, Russia). The illuminator scheme also contained beam splitter (*12*), protective optical filters (*13*), and auxiliary ocular (*14*), which were used for adjusting the system for formation of force laser beams. The radiation power incident on the cell was 0.5 – 1 mW.

Particles were observed with the help of objective (*6*) ($40^{\times}$, NA = 0.65) mounted in the microscope turret and MFN-11 microphotoadapter (*8*) (LOMO, Russia) allowing the visual observation of images through oculars (*9*) or recording them with digital Coolpix 4300 camera (*10*) (Nikon Corp., Japan). Radiation from the force laser was suppressed with SZS 22 glass filter (*7*) used in the optical scheme of the microscope.

The mechanical part of the system provides the independent movement of the force laser beam, the illuminating system, and the microcell with respect to microscope objective (*6*). For this purpose, objective (*3*) is placed on a horizontal dual-axis translation stage, which is mounted on a precision lifting platform providing vertical

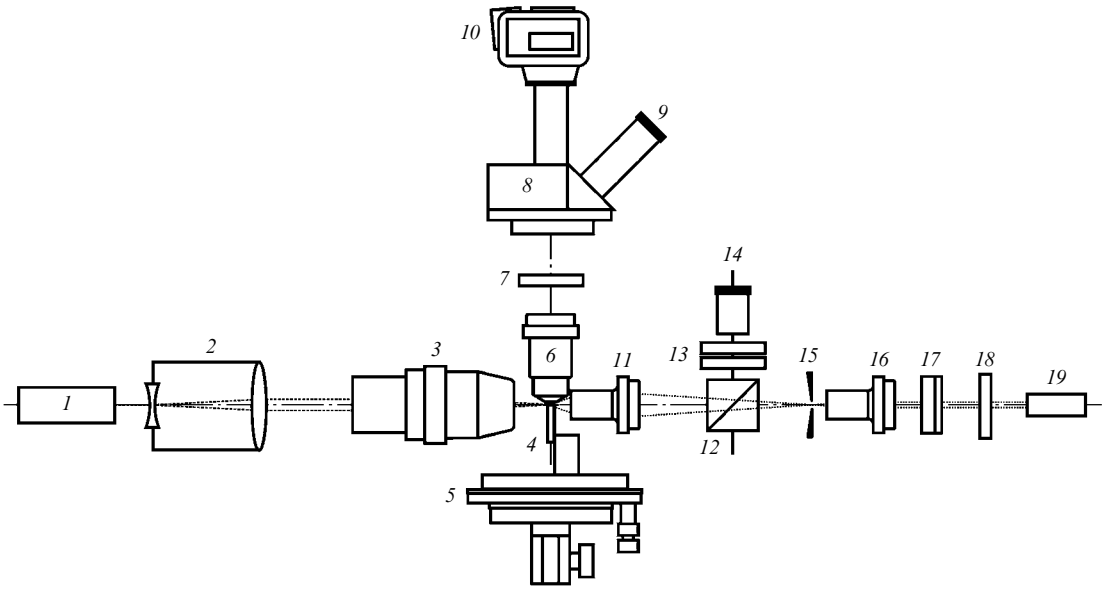

Figure 2. Scheme of a laser ultramicroscope: (*1*) force laser; (*2*) beam expander; (*3*) objective ($10^{\times}$, NA = 0.3); (4) microcell; (*5*) microscope stage; (*6*) microscope objective ($40^{\times}$, NA = 0.65); (*7*) optical filter suppressing force laser radiation; (*8*) microphotoadapter; (*9*) ocular; (*10*) digital chamber; (*11*) objective ($10^{\times}$, NA = 0.3); (*12*) beamsplitter; (*13*) protective optical filters; (*14*) auxiliary ocular; (*15*) controllable slit aperture; (*16*) objective ($8^{\times}$, *NA* = 0.2); (*17*) cylindrical lens; (*18*) optical filter; (*19*) illuminating laser.

positioning with a resolution of 1 μm. The cell was mounted on three-axis microscope stage (*5*). The illuminating system could be displaced as a whole along three axes on the adjustable base.

2.4 Image recording and processing

Images of moving particles were recorded with a digital camera operating in the video image translation regime and digitised with an image capture board (AverMedia, Russia) in a PC. The frame rate was 27 frames s^{-1} and the image size was 720×576 pixels (PAL standard). The linear field of view of the system for the maximum and minimum magnification of the microphotoadapter was 102×82 μm and 231×186 μm, respectively. The image capture and subsequent analysis by the PIV method were performed by using a software package that we developed in the Matlab 7.0 media (The Mathworks Inc., USA). The realisation volume used for the construction of the velocity field of particles was usually 500 video signal frames, which were stored in the JPEG format in a hard disc with the minimal compression. If necessary, a certain fragment was cut out from each of these images, which was then analysed with a high resolution.

The velocity field was analysed from the stored images by the PIV method by averaging correlation functions. Because images were recorded after equal time intervals, 499 pairs of frames were used totally to estimate the correlation function (the first and second frames, the second and third frames, etc.). The velocity field of particles obtained in this way was preserved in a tabular form of data in the text format.

3. Results and discussion

The results presented in this paper were obtained for the aqueous suspension of colloidal gold particles of diameter 40 nm. The extinction maximum for these particles is located at a wavelength of 550 nm, the absorption of light in the plasmon resonance band exceeding scattering [2]. This provides the efficient action of the 532-nm force laser radiation on particles, whereas the wavelength 660 nm of the illuminating laser is located outside the resonance absorption band. Figure 3 shows images of these particles illuminated by the laser ultramicroscope illuminator. The arrow indicates the plane optically conjugated with the telescopic slit of the illuminator system. Due to the use of an objective with a numerical aperture of 0.3 in the optical scheme of the illuminator, for the slit of width 10 μm the laser beam cross section had the form of a prolate ellipse with a major axis of length ~ 40 μm lying in the figure plane and a minor axis of length ~ 2 μm. The cross section of the illuminator beam was measured by directing the beam to microscope objective (*6*) after reflection from the hypotenuse face of a triangle glass prism placed on the microscope stage instead of the cell. Figure 3 demonstrates a decrease in the particle image contrast to the left and right of the slit image plane with increasing the beam diameter, which is caused by the scattering of light by particles outside the object plane of the microscope. Astigmatism introduced by a cylindrical lens leads to the narrowing of the laser beam, which is observed near the left edge of the figure where the beam cross section has the form of a prolate ellipse with the major axis perpendicular to the figure plane.

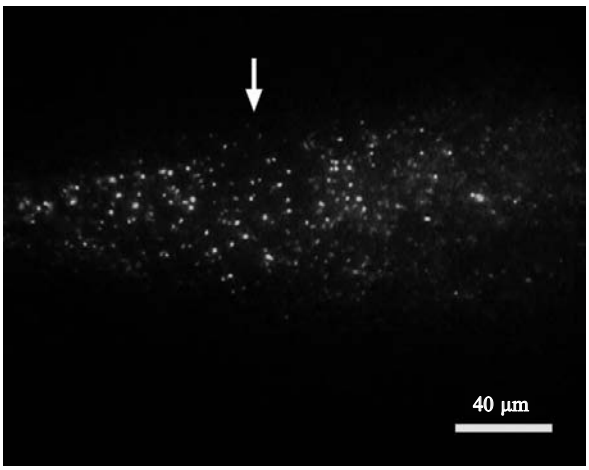

Figure 3. Images of colloidal gold particles of diameter 40 nm in the beam of a laser ultramicroscope illuminator. The arrow indicated the plane optically conjugated with a variable slit of the illuminator system.

Particles were observed by using a $40^{\times}$ objective with a numerical aperture of 0.65 and a working distance of 0.61 mm. A large working distance is required for studying flows formed in a closed cell at a considerable distance from the cell walls. The transverse size of images of point sources obtained with this objective and recalculated to the object plane was 1.1 μm and the depth of focus was ~ 4 μm [11]. The illumination of particles by a focused astigmatic beam provides the increase in the resolution over depth to 2 μm in a small region near the slit image plane and also enhances the image contrast.

Figure 4a shows the velocity field of particles moving in a 55-mW laser beam obtained by the PIV method. The waist diameter of the focused laser beam was 10 μm. The arrows show the propagation direction of particles, the arrow length corresponding to the average velocity of particles. This field was constructed by using an image fragment of size 200×200 pixels obtained with a resolution of 0.33 μm$\times$ pixel^{-1}. The correlation analysis was performed for 702 overlapping windows of size 30×10 pixels (along the x and y axes, respectively). The windows were overlapped by 20 and 5 pixels along the x and y axes, respectively. The spatial resolution, by neglecting the overlap of windows, was 10 μm along the x axis and 3 μm along the y axis. The coordinates of the origin of each velocity vector in Fig. 4a correspond to the position of the centre of the corresponding window in the initial frame.

In the plane conjugate to the slit image (shown by the dashed straight line in Fig. 4a), the transverse size of the illuminating beam is 2 μm, which allows us to study the transverse distribution of particle velocities in the laser beam with a high spatial resolution. Figure 4b shows the transverse distribution of particle velocities in this plane obtained by scanning the force laser beam along the vertical. Scanning was performed by moving objective (*3*) with a step of 3 μm (Fig. 2).

This distribution was constructed by recording 14 realisations corresponding to different positions of the force laser beam. Figure 4a shows the velocity field of particles calculated by the realisation corresponding to $z = 18$ μm. The transverse distribution of particle velocities corresponds to the laser beam intensity distribution repeating the

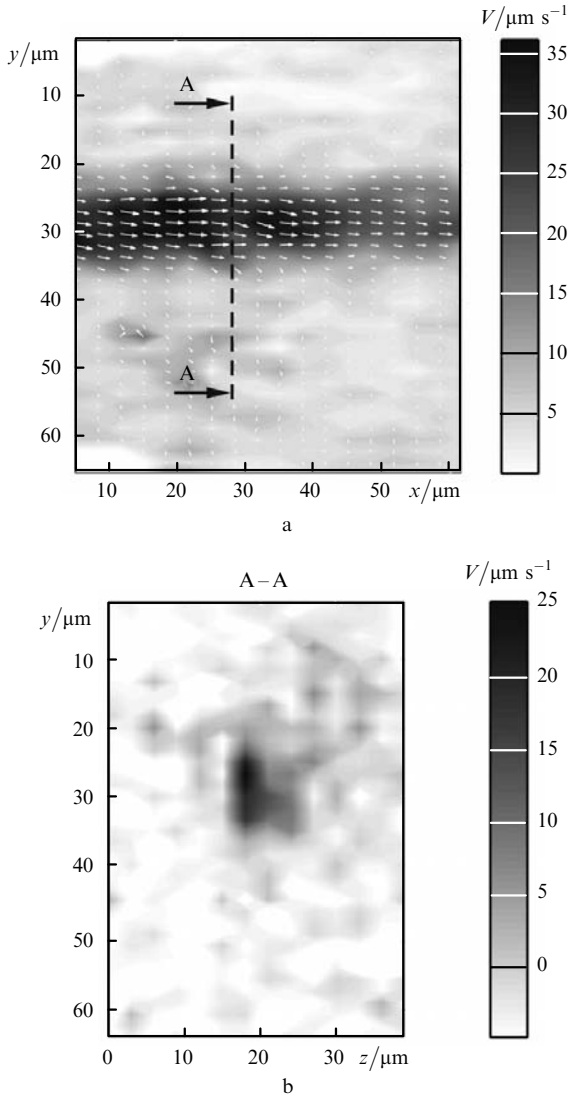

Figure 4. Velocity field of nanoparticles moving along the laser beam (a) and the transverse velocity distribution in the A – A section (b). The arrows show the propagation direction of particles; the arrow length and grey scale correspond to the average velocity of particles.

rectangular shape of the emitting area of a laser diode used as the force laser.

Particles were irradiated in the scheme considered above simultaneously by two counterpropagating laser beams. Radiation of each of the beams exerted pressure on particles in the cell. Pressure experienced by a particle in a cw laser beam is directly proportional to the ratio of the radiation power to the cross-sectional area of the laser beam. We studied the dependence of the velocity of particles on the laser beam axis on the radiation power incident on the cell. The output power of the force laser was controlled with the help of a rotating polarisation filter and measured with a Model 1815 power meter (Newport Corp., USA) at the input to an objective focusing radiation to the cell. The focused laser beam had the waist of diameter 10 μm. The beam axis of the illuminating laser was adjusted accurately along the force laser beam axis. The velocity field was calculated from frames of size 200 × 200 pixels. In the field obtained in this way, the average value of the x components of velocity vectors lying on the laser beam axis was calculated. Figure 5 presents the dependence of the particle

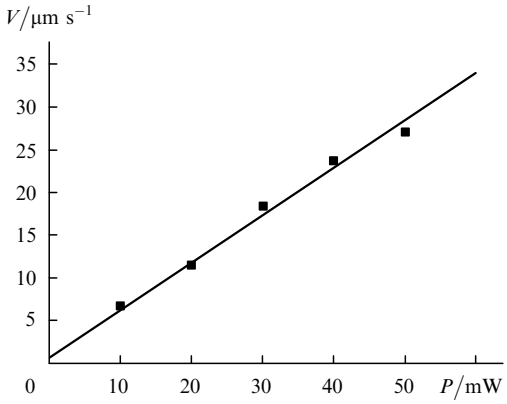

Figure 5. Dependence of the average velocity of particles on the laser beam axis on the laser radiation power. Squares are experimental results, the straight line is the linear regression.

velocity V on the laser radiation power P. One can see that the particle velocity is directly proportional to the output laser power.

The power of the illuminating laser beam in our experiments did not exceed 1 mW. The cross-sectional area in the waist of diameter 10 μm for the force laser beam was 8×10^{-7} mm^2, while the cross-sectional area of the illuminating laser beam in the form of an ellipse with axes 2 and 40 μm was 6×10^{-7} mm^2. Because these areas are of the same order of magnitude, the light pressure exerted by the 1-mW illuminating laser beam in its smallest cross section is 2 % – 10 % of the pressure exerted by the force laser radiation, which for small velocities of particles is considerably lower than the error introduced by Brownian motion.

4. Conclusions

The spatial resolution of most optical visualisation methods is limited by the wavelength of light, which considerably exceeds the size of colloidal particles. Despite this restriction, the application of optical methods for visualisation of colloidal systems is most promising for biological and medical investigations because only optical methods, which have the resolution sufficient for studying individual cells, exert the minimal effect on living organisms, which makes it possible to perform real-time studies.

In this paper we have considered the optical method for studying colloidal systems, which combines the force action on colloidal particles and visualisation of their dynamics. This method can be used for studying the interaction of colloidal particles with optical radiation and the environment. Due to its almost noninvasive nature, the method can be applied in microscopic studies of the fundamental mechanisms of interaction of contrasting and therapeutic agents based on colloidal particles with individual cells, for investigating mechanisms of transmembrane transfer of colloidal particles, processes of photothermal action on individual cells, and formation of clusters of colloidal particles in the laser radiation field.

Acknowledgements. This work was supported by Grants CRDF REC-006/SA-006-00 and BRHE RUXO-006-SR-06/BP1M06, the Federal Education Agency of the Russian Federation (Grant No. 1.4.06), and Grant No. RNP.2.1.4473.

References

1. Loo C., Lin A., Hirsch L., Lee M.-H., Barton J., Halas N., West J., Drezek W. *Technol. Cancer Res. Treat.*, **3** (1), 33 (2004).
2. Oldenburg S.J., Schultz D.A., in *Topics in Fluorescence Spectroscopy. Vol. 8: Radiative Decay Engineering* (New York: Springer Science, Business Media Inc., 2005).
3. Khlebtsov B.N., Zharov V.P., Melnikov A.G., Tuchin V.V., Khlebtsov N.G. *Nanotechnology*, **17** (20), 5167 (2006).
4. Kalele S., Gosavi S.W., Urban J., Kulkarni S.K. *Current Science*, **91** (8), 1038 (2006).
5. Siedentopf H., Zsigmondy R. *Annalen der Physik*, **10**, 1 (1903).
6. Molloy J.E., Dholakia K., Padgett M.J. *J. Mod. Opt.*, **50**, 1501 (2003).
7. Neuman K.C., Block S.M. *Rev. Sci. Instr.*, **75** (9), 2787 (2004).
8. Seol Y., Carpenter A.E., Perkins T.T. *Opt. Lett.*, **31** (16), 2429 (2006).
9. Fedosov I.V., Nefedov I.S., Khlebtsov B.N., Tuchin V.V. *Proc. SPIE Int. Soc. Opt. Eng.*, **6536**, DOI: 10.1117/12.753444 (2007).
10. Fedosov I.V., Nefedov I.S., Khlebtsov B.N., Tuchin V.V. *SPIE Newsroom*, http://spie.org/x14817.xml?highlight=x2400, DOI: 10.1117/2.1200706.0803 (2007).
11. Wereley S.T., Meinhart C.D., in *Microscale Diagnostic Techniques* (Berlin, Heidelberg, New York: Springer, 2005) p. 51.
12. Park J.S., Kihm K.D. *Exp. Fluids*, **40**, 491 (2006).
13. Krylov V.A., Lazukina O.P., Ketkova L.A., Bulanov A.D., Adamchik S.A., Kobyshcha D.G. *Zh. Analit. Khim.*, **55**, 326 (2000).
14. Chernoberezhskii Yu.M., Rudakova I.S., Lorentsson A.V. *Kolloid. Zh.*, **69**, 261 (2007).
15. Dodt H.-U., Leischner U., Schierloh A., Jahrling N., Mauch C.P., Deininger K., Deussing J.M., Eder M., Zieglgansberger W., Becker K. *Nature Methods*, **4** (4), 331 (2007).
16. Adrian R.J. *Ann. Rev. Fluid Mechanics*, **23**, 261 (1991).
17. Meinhart C.D., Wereley S.T., Santiago J.G. *J. Fluids Eng.*, **122**, 285 (2000).
18. Probstein R.F. *Physicochemical Hydrodynamics: An Introduction* (New York: John Wiley & Sons, 1994).
19. Einstein A., in *Theory of Brownian Movement* (New York: Dover Publ. Inc., 1905) p. 1.
20. Devasenathipathy S., Santiago J.G., Wereley S.T., Meinhart C.D., Takehara K. *Exp. Fluids*, **34**, 504 (2003).